Anal. Chem. **2002,** *74,* 6006−6016

Simulation of Packed-Bed Chromatography Utilizing High-Resolution Flow Fields: Comparison with Models

Mark R. Schure*

Theoretical Separation Science Laboratory, Rohm and Haas Company, 727 Norristown Road, Box 0904, Spring House, Pennsylvania 19477-0904

Robert S. Maier

Army High Performance Computing Research Center, University of Minnesota, 1100 Washington Avenue South, Minneapolis, Minnesota 55415

Daniel M. Kroll

Department of Medicinal Chemistry and Minnesota Supercomputer Institute, University of Minnesota, 599 Walter Library, 117 Pleasant Street S.E., Minneapolis, Minnesota 55455

H. Ted Davis

Department of Chemical Engineering and Materials Science, University of Minnesota, Amundson Hall, 421 Washington Avenue S.E., Minneapolis, Minnesota 55455

A computer simulation of a section of the interior region of a liquid chromatographic column is performed. The detailed fluid flow profile is provided from a microscopic calculation of low Reynolds number flow through a random packed bed of nonporous spherical particles. The fluid mechanical calculations are performed on a parallel processor computer utilizing the lattice Boltzmann technique. Convection, diffusion, and retention in this flow field are calculated using a stochastic-based algorithm. This computational scheme provides for the ability to reproduce the essential dynamics of the chromatographic process from the fundamental considerations of particle geometry, particle size, flow velocity, solute diffusion coefficient, and solute retention parameters when retention is utilized. The simulation data are fit to semiempirical models. The best agreement is found for the "coupling" model of Giddings and the four-parameter Knox model. These models are verified over a wide range of particle sizes and flow velocities at both low and high velocity. The simulations appear to capture the essential dynamics of the chromatographic flow process for nondimensional flow velocities (Péclet number) less than 500. Since the same packing geometry is utilized for different particle size studies, the interpretation of the parameter estimates from these models can be extended to the physical column model. The simulations reported here agree very well with a number of experiments reported previously.

Liquid chromatography is an indispensable method for the separation of many types of molecules.[1,2] The knowledge required for a fundamental in-depth understanding of this technique resides in two distinctly different aspects. The first of these aspects is the interaction of the solute molecules with the "stationary" or "retentive" phase, resulting in differing mean molecular residence times at the surface, according to the solute molecular structure. Various models have been proposed for these interactions.[3−6] These models are obtained via thermodynamic-based measurements that due to the fundamental limitations of thermodynamics cannot be extrapolated to give a molecular-level picture. The second aspect is the flow mechanics of the solutes as separation proceeds through the combined effects of retention, diffusion, and convection.[7,8]

Fundamental information regarding the first aspect has been obtained through a number of experimental methods that can

* Corresponding author. E-mail: mschure@rohmhaas.com.

(1) Snyder, L. R.; Kirkland, J. J. *Introduction to Modern Liquid Chromatography*; John Wiley and Sons: New York, 1979.
(2) *High Performance Liquid Chromatography of Peptides and Proteins: Separation, Analysis, and Conformation*; Mant, C. T., Hodges, R. S., Eds.; CRC Press: Boca Raton, FL, 1991.
(3) *Retention and Selectivity in Liquid Chromatography: Prediction, Standardization, and Phase Comparisons*; Smith, R. M., Ed.; Elsevier Publishing: New York, 1995.
(4) Vailaya, A.; Horváth, C. *J. Phys. Chem. B* **1997**, *101*, 5875−5888.
(5) Vailaya, A.; Horváth, C. *J. Chromatogr., A* **1998**, *829*, 1−27.
(6) Ranatunga, R. P. J.; Carr, P. W. *Anal. Chem.* **2000**, *72*, 5679−5692.
(7) Giddings, J. C. *Dynamics of Chromatography*; Marcel Dekker: New York, 1965.
(8) Knox, J. H. In *Advances In Chromatography*; Brown, P. R., Grushka, E., Eds.; Marcel Dekker Publishing: New York, 1998; Vol. 38, pp 1−49.

10.1021/ac0204101 CCC: $22.00
Published on Web 11/01/2002

study the stationary phase and in some cases the interactions of the solute with the stationary phase. These techniques include NMR,[9−11] IR,[12] and fluorescence.[13−15] Although there are many questions regarding the retention mechanisms in liquid chromatography, many of these questions have been answered and it is the challenge of experimental and simulation techniques to further refine these mechanisms and make them quantitative.

Fundamental information regarding the fluid mechanical aspects of the packed-bed chromatographic experiment have largely been developed along two lines of research that include fundamental engineering studies of flow through porous media[16−18] and the development of porous media flow studies specifically oriented toward chromatography.[7,8,19−24] In both cases, experimental studies of the detailed microhydrodynamics have been difficult to conduct because the usual method of measuring the peak broadening of a tracer solute through zone shape analysis offers little insight into the process. Theoretical models of zone broadening have been largely constructed through comparison with this type of experiment. Recently, the use of fluorescence[25,26] and NMR[27−32] have provided additional insight into the flow in porous media problem and chromatographically relevant studies. Furthermore, flow visualization studies[33−35] have been used recently to study tracer dispersion in porous media, yielding some additional information regarding the extent of the dispersive process. This visualization technique is very powerful because one can study localized regions of columns. This is difficult to conduct because image reconstruction methods are needed to undo the signal summation that typically takes place in both the cross-sectional and axial spatial directions. One of the most important results of this line of research has been the discovery of wall effects[34] in chromatographic columns. Wall effects have also been revealed by dynamic NMR techniques.[36−38]

Through advances in numerical algorithm research and computer hardware technology it is now possible to calculate the complete flow field in a reasonably large packed bed of particles. This allows an extra level of insight that cannot be provided by current experiments. Specifically, these advances involve the development and utilization of the lattice Boltzmann (LB) technique,[39−41] which is capable of accurate calculation of flow fields in the low Reynolds number region using parallel computers. Parallel computing is essential in porous flow simulations in order to perform the simulation in a reasonable amount of time. Parallel computation is also necessary to efficiently utilize the large amounts of memory that are necessary because of the fine numerical grid required to achieve accurate simulations.

A number of computer simulation studies of porous media flow have been conducted over the last five years.[42−47] These simulations offer a very accurate way to calculate fluid velocities at all spatial locations within the porous media space for the low Reynolds number flows pertinent to chromatography. The accuracy of the calculation is typically tied to the spatial resolution of the computational grid. Hence, larger memory machines, more processors, or both are required to accurately resolve the details of the flow field.

A number of studies have recently focused on tracer dispersion.[44−50] Some of these studies have considered dispersive effects in packed beds modeled as an assembly of capillaries or some other simplified connective model,[48−50] but these models miss some of the essential ingredients such as the eddy or mechanical dispersion effects that are central to the packed-bed chromatographic problem.

(9) Albert, K.; Bayer, E. *J. Chromatogr.* **1991**, *544*, 345−370.
(10) Ziegler, R. C.; Maciel, G. E. *J. Am. Chem. Soc.* **1991**, *113*, 6349−6358.
(11) Sentell, K. B.; Bliesner, D. M.; Shearer, S. T. In *Chemically Modified Surfaces*; Pesek, J. J., Leigh, I. E., Eds.; Royal Society of Chemistry: Cambridge, England, 1994; pp 190−202.
(12) Sander, L. C.; Callis, J. B.; Field, L. R. *Anal. Chem.* **1983**, *55*, 1068−1075.
(13) Lochmüller, C. H.; Colborn, A. S.; Hunnicutt, M. L.; Harris, J. M. *Anal. Chem.* **1983**, *55*, 1344−1348.
(14) Bogar, R. C.; Thomas, J. C.; Callis, J. B. *Anal. Chem.* **1984**, *56*, 1080−1084.
(15) Hansen, R. L.; Harris, J. M. *Anal. Chem.* **1996**, *68*, 2879−2884.
(16) Bear, J. *Dynamics of Fluids in Porous Media*; Dover Publications Inc.: New York, 1988.
(17) *Dynamics of Fluids in Hierarchical Porous Media*; Cushman, J. H., Ed.; Academic Press: New York, 1990.
(18) Adler, P. M. *Porous Media: Geometry and Transports*; Butterworth-Heinemann: Stoneham, MA, 1992.
(19) van Deemter, J. J.; Zuiderweg, F. J.; Klinkenberg, A. *Chem. Eng. Sci.* **1956**, *5*, 271−289.
(20) Horváth, C.; Lin, H.-J. *J. Chromatogr.* **1978**, *149*, 43−70.
(21) Weber, S. G.; Carr, P. W. In *High Performance Liquid Chromatography*; Brown, P. R., Hartwick, R. A., Eds.; John Wiley and Sons: New York, 1989.
(22) Magnico, P.; Martin, M. *J. Chromatogr.* **1990**, *517*, 31−49.
(23) Knox, J. H.; Laird, G. R.; Raven, P. A. *J. Chromatogr.* **1976**, *122*, 129−145.
(24) Knox, J. H. *J. Chromatogr., A* **1999**, *831*, 3−15.
(25) Northrup, M. A.; Kulp, T. J.; Angel, S. M.; Pinder, G. F. *Chem. Eng. Sci.* **1993**, *48*, 13−21.
(26) Rashidi, M.; Peurrung, L.; Tompson, A. F. B.; Kulp, T. J. *Adv. Water Resour.* **1996**, *1*, 163−180.
(27) Banavar, J. R.; Schwartz, L. M. In *Molecular Dynamics in Restricted Geometries*; Klafter, J., Drake, J. M., Eds.; John Wiley and Sons: New York, 1989.
(28) Lebon, L.; Oger, L.; Leblond, J.; Hulin, J. P.; Martys, N. S.; Schwartz, L. M. *Phys. Fluids* **1996**, *8*, 293−301.
(29) Tallarek, U.; Bayer, E.; Guiochon, G. *J. Am. Chem. Soc.* **1998**, *120*, 1494−1505.
(30) Yuan, Q. S.; Rosenfeld, A.; Root, T. W.; Klingenberg, D. J.; Lightfoot, E. N. *J. Chromatogr., A* **1999**, *831*, 149−165.
(31) Tallarek, U.; Vergeldt, F. J.; Van As, H. *J. Phys. Chem. B* **1999**, *103*, 7654−7664.
(32) Tallarek, U.; Rapp, E.; Scheenen, T.; Bayer, E.; Van As, H. *Anal. Chem.* **2000**, *72*, 2292−2301.
(33) Broyles, B. S.; Shalliker, R. A.; Guiochon, G. *J. Chromatogr., A* **2000**, *867*, 71−92.
(34) Shalliker, R. A.; Broyles, B. S.; Guiochon, G. *J. Chromatogr., A* **2000**, *888*, 1−12.
(35) Shalliker, R. A.; Broyles, B. S.; Guiochon, G. *Anal. Chem.* **2000**, *72*, 323−332.
(36) Sederman, A. J.; Alexander, P.; Gladden, L. F. *Powder Technol.* **2001**, *117*, 255−269.
(37) Tallarek, U.; Scheenen, T. W. J.; Van As, H. *J. Phys. Chem. B* **2001**, *105*, 8591−8599.
(38) Park, J. C.; Raghavan, K.; Gibbs, S. J. *J. Chromatogr., A* **2002**, *945*, 65−81.
(39) McNamara, G. R.; Zanetti, G. *Phys. Rev. Lett.* **1988**, *61*, 2332−2335.
(40) Higuera, F.; Jimenez, J. *Europhys. Lett.* **1989**, *9*, 663−668.
(41) Succi, S.; Benzi, R.; Higuera, F. In *Lattice Gas Methods: Theory, Applications, and Hardware*; Doolen, G., Ed.; Elsevier: Amsterdam, 1991; pp 219−230.
(42) Lebon, L.; Oger, L.; Leblond, J.; Hulin, J. P.; Martys, N. S.; Schwartz, L. M. *Phys. Fluids* **1996**, *8* (2), 293−301.
(43) Maier, R. S.; Kroll, D. M.; Kutsovsky, Y. E.; Davis, H. T.; Bernard, R. S. *Phys. Fluids* **1998**, *10* (1), 60−74.
(44) Tessier, J. J.; Packer, K. J.; Thovert, J.-F.; Adler, P. M. *AIChE J.* **1997**, *43* (7), 1653−1661.
(45) Coelho, D.; Thovert, J.-F.; Adler, P. M. *Phy. Rev. E* **1997**, *55*, 1959−1978.
(46) Maier, R. S.; Kroll, D. M.; Davis, H. T.; Bernard, R. S. *Int. J. Mod. Phys. C* **1998**, *8*, 1523−1533.
(47) Maier, R. S.; Kroll, D. M.; Bernard, R. S.; Howington, S. E.; Peters, J. F.; Davis, H. T. *Phys. Fluids* **2000**, *12* (8), 2065−2079.
(48) Meyers, J.; Liapis, A. I. *J. Chromatogr., A* **1998**, *827*, 197−213.
(49) Matsuyama, H.; Teramoto, M.; Suzuki, K. *Sep. Sci. Technol.* **1997**, *32*, 2439−2366.
(50) Martys, N. S. *J. Chromatogr., A* **1995**, *707*, 35−43.

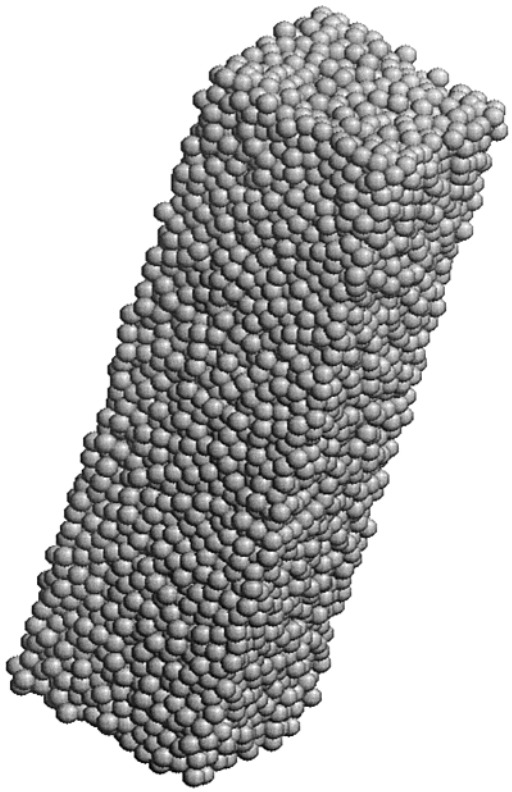

Figure 1. Particle pack used in these calculations. The periodic image of particles, which intersect a face boundary, has been added to the particle pack in this figure.

In this paper, we present the results of a detailed study of the chromatographic process obtained by conducting simulations of solute diffusion and convection in the flow field of a packed bed with a geometry typical of that used in liquid chromatography. Retention is not included in this study. However, we describe how it can be easily incorporated into the simulation. These results, which produce peak shapes typical of chromatographic zones, are used to determine the dispersion (plate height) versus flow velocity plots, which can be directly analyzed using previously derived chromatographic theory. By comparison with these models, it will be demonstrated that the semiempirical four-parameter model of Knox and the semiempirical coupling model of Giddings provide a quantitatively accurate estimation of zone broadening in liquid chromatography over a wide parameter range.

COMPUTATIONAL PROCEDURES

Flow Field Calculations. The details of the calculation of the flow fields are given elsewhere,[43,46] but the essential elements are presented here for clarity. Spheres are randomly packed into a rectangular box with the volume fraction of spheres, ϕ, approximately equal to 0.64. This is the volume fraction of a "randomly packed"[51,52] box and corresponds to a porosity $\epsilon = 1 - \phi = 0.36$, which may be found in a chromatographic column. The particle pack used here is shown in Figure 1.

The packing algorithm used here is similar to other packing algorithms[53−55] and utilizes a parallel Monte Carlo algorithm. Spheres are arranged initially in a dilute cubic array within a periodic domain with dimensions twice that of the target box. Each sphere was moved in a random direction, and the move was accepted if it did not result in a collision with the wall boundary or another sphere. After a series of such Monte Carlo steps, the coordinate system is scaled while constant sphere diameter is maintained. This procedure is repeated with an apparent exponential convergence to the desired density. Although recent techniques have appeared in the literature to quantify order or local crystallinity in sphere packs,[56] visual inspection of the resulting sphere pack showed little signs of crystallinity.

No attempt is made to model the particle packing process that is used in column manufacturing. Modeling of this process has recently been reported for microcolumns,[57] and these simulations gave higher porosity values than used here but well within the range typically found for chromatographic columns.[58] All particles packed in the current study are spherical and nonporous. Extension of the results given here to porous particles will be reported in a separate paper.

Periodic boundary conditions[59,60] are used in both the flow calculations and the particle packing algorithms so that the flow and solute movement do not hit a vapor−liquid or vapor−solid interface during the simulation process. The simulations reported here are therefore strictly limited to the interior of the column and do not include any wall effects[34] that exist in the total column fluid mechanics. Furthermore, the use of periodic boundaries facilitates the study of longer physical domains by allowing for the solute to reenter the packed box in the opposite face after leaving the box.

The flow field is calculated using the 15-point LB method as described previously.[43] These calculations are run on a 64 processor IBM SP parallel processor supercomputer (Armonk, NY). The version of the LB method used here is second order accurate in the bulk fluid region between surfaces and first order accurate at the surface of the particles.[43] For the study reported here, we use a particle pack made with 4000 particles with grid dimensions of 256 by 256 by 1024 in *x*, *y*, and *z* directions, respectively, where *z* is the axial coordinate. Each sphere has a diameter of 27.37 lattice points. This large box size minimizes tracer recorrelation due to periodic boundaries, an effect that has been studied in previous investigations of tracer dispersion.[47]

The Reynolds number is sufficiently low for these calculations that inertial effects are minimal. This flow regime is referred to as creeping flow.[61,62] We take advantage of this by calculating one

(51) German, R. M. *Particle Packing Characteristics*; Metal Powder Industries Federation: Princeton, NJ, 1989.
(52) Torquato, S.; Truskett, T. M.; Debenedetti, P. G. *Phys. Rev. Lett.* **2000**, *84*, 2064−2067.
(53) Jodrey, W. S.; Tory, E. M. *Phys. Rev. A* **1985**, *32*, 2347−2351.
(54) Soppe, W. *Powder Technol.* **1990**, *62*, 198−196.
(55) He, D.; Ekere, N. N.; Cai, L. *Phys. Rev. E* **1999**, *60*, 7098−7104.
(56) Truskett, T. M.; Torquato, S.; Debenedetti, P. G. *Phys. Rev. E* **2000**, *62*, 993−1001.
(57) Vissers, J. P. C.; Hoeben, M. A.; Laven, J.; Claessens, H. A.; Cramers, C. A. *J. Chromatogr., A* **2000**, *883*, 11−25.
(58) Guiochon, G.; Shirazi, S. G.; Katti, A. M. *Fundamentals of Preparative and Nonlinear Chromatography*; Academic Press: New York, 1994.
(59) Allen, M. P.; Tildesley, D. J. *Computer Simulation of Liquids*; Oxford Science Publications: New York, 1987.
(60) Frenkel, D.; Smit, B. *Understanding Molecular Simulation*; Academic Press: San Diego, CA, 1996.
(61) White, F. M. *Viscous Fluid Flow*; McGraw-Hill Inc.: New York, 1991.
(62) Leal, L. G. *Laminar Flow and Convective Transport Processes*; Butterworth-Heinemann Publishing: Boston, MA, 1992.

flow field for a given pack, and all other flows are obtained from this one flow field by linear scaling. The base flow field from which other velocities are obtained by scaling is run at a Reynolds number of 0.005. The accuracy of this procedure is discussed in the Results section below.

After the calculation of the flow field, which gives the fluid vector velocities in the *x*, *y*, and *z* directions at each point in the computational grid, these velocities are stored in disk files for later retrieval during the stochastic particle simulation, described below. Note that the velocity field is equal to zero inside the particle and at the particle surface because no-slip boundary conditions are used in the LB calculations.

Convection, Diffusion, and Retention. After the flow field velocities are read from the disk, linear interpolation coefficients are calculated for the *x*, *y*, and *z* components between each grid point. These coefficients have the trilinear hexahedral element functional form typically used in finite element modeling:[63]

$$v_u = a_{0,u} + a_{1,u}x + a_{2,u}y + a_{3,u}z + a_{4,u}xy + a_{5,u}xz + a_{6,u}yz + a_{7,u}xyz \quad (1)$$

where u is one of the spatial coordinates, i.e., $u = x$, y, or z, and v_x, v_y, and v_z are the fluid velocities in the *x*, *y*, and *z* directions at each specified location. The eight coefficients are obtained with an eight-point cube of local flow velocities. The calculation of the coefficients is done using a simple matrix solution.[63,64]

The convection, diffusion, and retention algorithm is based on a stochastic technique[65] that writes the arrival time of a solute molecule at a specified column length L to disk. These arrival times are used to compute an arrival time histogram that is transformed into a concentration profile.

The stochastic simulation of the chromatographic process starts by placing a solute molecule at the front face at $z = 0$ with randomly chosen *x* and *y* coordinates not in a solid particle. The solute particle is then allowed to diffuse an average length $(2Dt_s)^{1/2}$ in each spatial coordinate, where D is the diffusion coefficient and t_s is the time step. This is based on the Einstein equation,[66,67] which gives the average distance $\bar{u}$ diffused in time t equal to $(2Dt)^{1/2}$ in one dimension. The actual diffusion algorithm used here generates Gaussian random numbers in each spatial dimension with standard deviation σ equal to $(2Dt_s)^{1/2}$. The generation algorithm is based on the polar method.[68] We use Gaussian random deviates, as also used in the diffusion processes of Brownian dynamics simulations,[59,60] instead of the uniform deviates previously used[65] in these types of simulations. This is done because in this complex boundary flow problem, where very narrow interstitial pore spaces exist, solute molecules have been stuck in infinite retention loop trajectories if simply moved by $\pm(2Dt_s)^{1/2}$ in each spatial coordinate. This problem never appeared when the Gaussian random values were used for diffusion.

If the solute particle's trajectory takes it into a solid particle, the solute particle's position is frozen and the time increment taken to diffuse into and from the surface is added to the time variable. That time increment is calculated as follows. The distance l between the solute starting position and the solid surface reached in three dimensions by diffusion is $(6Dt_s)^{1/2}$. Solving for t_s, and doubling it to get the time for diffusion to the surface and then back to the original position, $t'_s = l^2/3D$. This treatment simplifies the programming and also eliminates a truncation error of placing the solute a microscopic distance away from the surface. Since t_s is kept small so that $(6Dt_s)^{1/2} \ll d$, where d is the packing particle diameter, this treatment causes little distortion.

If penetration into a packing particle occurs, a counter that is associated with each solute particle is incremented so that the total number of surface associations is recorded throughout the solute particle's trajectory. In this way, retention phenomena are added after the simulation is completed. This is far more efficient because the retention phenomenon for the linear chromatography application studied here is independent of the mobile-phase fluid mechanics. In other words, individual retention events can be added after the elution time per particle is recorded. The description of how this is done has been provided by earlier work in the stochastic theory of chromatography,[69,70] where exponential waiting times derived from Poisson statistics[71−74] are added to the elution time for each surface collision.

Convection is modeled by the equation

$$u_{i+1} = u_i + v_u t_s \quad (2)$$

where u is again either *x*, *y*, or *z* and the subscript i refers to the iteration number. The value of v_u is calculated from eq 1. The 24 interpolation coefficients used for the calculation of v_x, v_y, and v_z are chosen through indexing on the present position values u_i. The convection and diffusion process is repeated until the particle position equals or exceeds the column length L. The output data include the exit radial position, the arrival time, and the number of surface associations of each particle.

Machine Implementation. The parallel computer elution profile simulations have not been described previously. These are performed on a cluster of eight dual-processor computers (Dell model 530, Austin TX) utilizing Intel (Santa Clara, CA) Pentium 4 Xeon processors with 2.0-GHz clock speeds and one Dell model 330 single processor computer with clock speed of 1.5 GHz used as the master node. The master node, referred to here as node 0, manages the data flow of initial and final values to the other 16 processors that are utilized for computing the convection, diffu-

(63) Hughes, T. J. R. *The Finite Element Method*; Prentice Hall Inc.: Englewood Cliffs, NJ, 1987.

(64) Anderson, E.; Bai, Z.; Bischof, C.; Demmel, J.; Dongarra, J.; Du Croz, J.; Greenbaum, A.; Hammarling, S.; McKenney, A.; Ostrouchov, S.; Sorenson, D. *LAPACK User's Guide*; Society for Industrial and Applied Mathematics: Philadelphia, PA, 1992.

(65) Schure, M. R. In *Advances In Chromatography*; Brown, P. R.; Grushka, E., Eds.; Marcel Dekker Publishing: New York, 1998.; Vol. 39, pp 139−200.

(66) Einstein, A. *Investigations on the Theory of Brownian Motion*; Dover Publications: New York, 1956.

(67) Berg, H. C. *Random Walks in Biology*; Princeton University Press: Princeton, NJ, 1993.

(68) Press, W. H.; Teukolsky, S. A.; Vetterling, W. T.; Flannery, B. P. *Numerical Recipes*, 2nd ed.; Cambridge University Press: New York, 1992.

(69) Giddings, J. C.; Eyring, H. *J. Phys. Chem.* **1955**, *59*, 416−421.

(70) McQuarrie, D. A. *J. Chem. Phys.* **1963**, *38*, 437−445.

(71) Hughes, B. D. *Random Walks and Random Environments*; Oxford University Press: New York, 1995.

(72) Hamming, R. W. *Numerical Methods for Scientists and Engineers*, 2nd ed.; McGraw-Hill: New York, 1973.

(73) Devroye, L. *Non-Uniform Random Variate Generation*; Springer-Verlag Publishing: New York, 1986.

(74) Schure, M. R.; Lenhoff, A. M. *Anal. Chem.* **1993**, *65*, 3024−3037.

sion, and retention algorithm described above. The physical domain of the flow field is broken up into 16 pieces partitioned as 2 (x) by 2 (y) by 4 (z) blocks.

Each computer has 2 Gbytes of memory and 36 Gbytes of SCSI disk space. These are interconnected with a high-speed optical switch (3Com model 4900 SX, Santa Clara, CA) which provides 1 Gbit/s transfer with optical fiber interconnects. Each computer has a Netgear (Santa Clara, CA) model GA621 gigabit optical interface. The software is written in Fortran 90 utilizing the Portland Group, Inc. (Portland, OR) compiler. The operating system is version 7.2 of Red Hat Linux[75] with version 2.4.17 of the operating system kernel. Interprocess communication is handled by the message passing interface (MPI) protocol.[76,77] A flowchart of the parallel program is shown in Figure 2.

Upon program activation, nodes 1−16 read the individual section of flow field interpolants from a disk on each processor, as shown in Figure 2. Node 0 then computes the initial starting position in the $z = 0$ plane, as discussed above. These positions are then sent to the appropriate processor. Node 0 receives the particles as they pass the column length L, and when all particles have been sent back to node 0, the new velocity scalings are computed and new initial conditions are calculated. These initial positions are then sent to the appropriate nodes, and the simulation is continued. Note that we have the capability for simulating multiple channel lengths, but this complicates the flowchart and is not shown for clarity. After simulating all of the elution profiles that have been specified, the node 0 process sends a code to the other nodes, which shuts them down in an orderly manner.

Each grid point has 3 spatial interpolation coordinates and it takes 8 bytes per number and 8 numbers, as shown in eq 1, to hold an interpolant. This yields a total storage requirement of over 12 Gbytes. Partitioning this amount of storage into each of the 16 processors results in the utilization of >82% of each processor's memory. Benchmarks of the elution code have established that the processors are typically kept running >60% of the time with interprocess communication taking up the remaining time slice.

Data Treatment. The resulting arrival time data is converted into plate height H and reduced plate height h via the following treatment. The first moment, M_1, and the second moment, M_2, of the arrival time distribution are calculated as

$$M_1 = \frac{1}{N}\sum_{i=1}^{N} t_i \tag{3}$$

where t_i is the arrival time of the ith particle, N is the number of particles, and

$$M_2 = \frac{1}{N}\sum_{i=1}^{N} (t_i - M_1)^2 \tag{4}$$

for the second moment. The plate height H and the reduced plate height h are then given as

$$H = LM_2/M_1^{\,2} \quad \text{and} \quad h = H/d \tag{5}$$

The velocities used for curve fitting are derived from cross-sectional averages of the flow in the z direction taken at three locations, $z/L = 0.2$, $z/L = 0.4$, and $z/L = 0.8$. These cross-sectional averages are then averaged to get the mean flow velocity v. The reduced velocity ν or Péclet number is calculated as $\nu = vd/D$.

Models and Curve Fitting. The seven empirical chromatographic models used for curve fitting h versus ν are similar to those used by Tallarek, Bayer, and Guiochon.[29] They are described briefly here, but a more detailed description of these models is available in ref 29 and in the original papers.

In the Giddings model of zone broadening,[7] a comprehensive approach is used that incorporates mechanical (eddy) dispersion, Taylor dispersion, intraparticle dispersion due to diffusion in the pore space, and mobile-phase dispersion due to molecular diffusion. The two variations of this model used here include the five-parameter model:

$$h = \frac{2\gamma}{\nu} + \frac{2\lambda}{1 + \omega\nu^{-n}} + c\nu \tag{6}$$

where γ is a tortuosity factor and λ and ω are so-called geometric parameters.[7,29] In eq 6, n is equal to 1 in the four-parameter model and is left as an undetermined parameter in the five-parameter model. The c term is due to mass transport resistances that include intraparticle pore space diffusion, which is not present here because we are modeling nonporous particles, and Taylor dispersion. We will refer to these models as G4 and G5.

The van Deemter equation[19] is a three-parameter relationship that has been utilized for many studies of zone broadening. It has the functional form

$$h = a + b/\nu + c\nu \tag{7}$$

The first term represents mechanical dispersion, the second term describes the effects of mechanical dispersion and molecular diffusion, and the third term describes mass transport resistances. This model will be referred to as vD3.

The Knox equation[8] is a simple modification of the van Deemter and Giddings equations:

$$h = a\nu^n + b/\nu + c\nu \tag{8}$$

where the first term describes the effect of mechanical dispersion, the second term describes molecular diffusion, and the third term describes mass transport resistances. The value of n is usually set to 1/3. This three-parameter model will be referred to as K3 and the four-parameter model, where n is a free variable, will be referred to as K4.

The Huber model has the same functional form as the four-parameter Giddings model, with the constraint that $n = 1/2$. We will refer to this model as H4. The Horváth and Lin model has

(75) http://www.redhat-linux.com.my/.

(76) Gropp, W.; Lusk, E.; Skjellum, A. *Using MPI: Portable Parallel Programming with the Message-Passing Interface*, 2nd ed.; MIT Press: Cambridge, MA, 1999.

(77) MPI information is available at http://www-unix.mcs.anl.gov/mpi/.

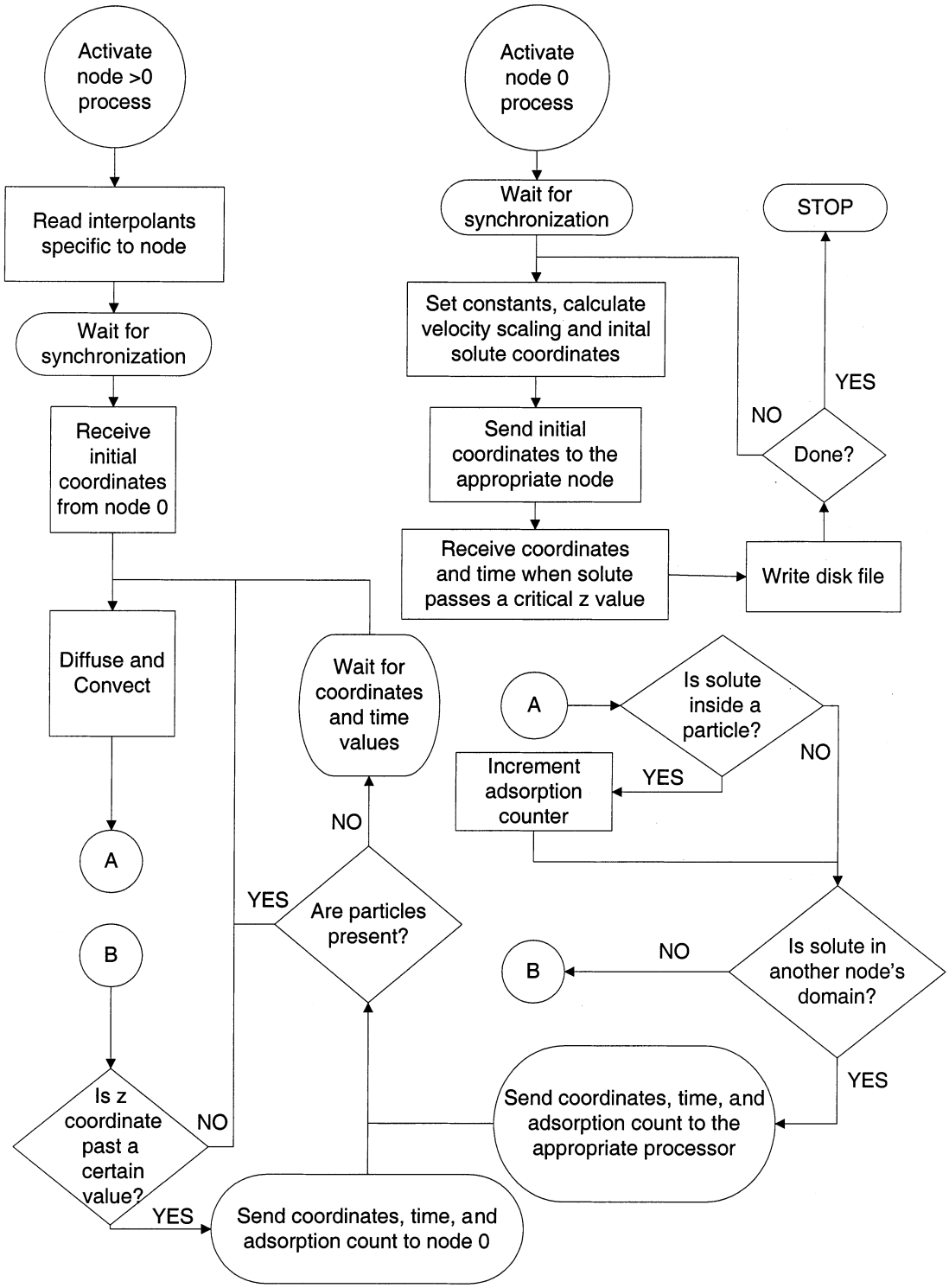

Figure 2. Flowchart of the elution process simulation.

the same functional form as the four-parameter Giddings model except that $n = 1/3$. We will refer to this model as HL4.

Curve fitting of the models to the h versus ν data is performed initially using simplex least-squares minimization,[78] to get good starting parameter estimates, followed by Levenberg−Marquardt least-squares minimization,[79] to get the final parameter estimates. These fits are done interactively because in some cases the initial estimates used in the simplex step yield inaccurate estimates, which then caused singular conditions to exist in the Levenberg−Marquardt step. This is likely due to the interdependence of parameters to be estimated, especially when exponential terms are present.

Parameter Ranges. The simulation results given in this paper are run over the range of conditions given in Table 1 and are

(78) O'Neill, R. In *Applied Statistics Algorithms*; Griffiths, P., Hill, I. D., Eds.; Ellis Horwood Limited: Chichester, England, 1985; pp 79−87.

(79) Bevington, P. R. *Data Reduction and Error Analysis for the Physical Sciences*; McGraw-Hill Book Co.: New York, 1969.

Table 1. Range of Parameters Utilized in the Simulations Given in This Paper

simulation	particle size (μm)	v range (cm·s^{-1})	ν range	Re range
1	9	1.00×10^{-5}−3.50×10^{-2}	0.1125−393.75	9.00×10^{-5}−0.315
2	50	2.00×10^{-6}−6.50×10^{-3}	0.125−406.25	1.00×10^{-4}−0.325
3	210	5.00×10^{-7}−1.40×10^{-3}	0.131−367.5	1.05×10^{-4}−0.294

Table 2. Flow Field Rescaling Error[a]

	rescaled velocity to a Reynolds number of			
starting Re	0.001	0.005	0.05	0.5
0.001		1.50×10^{-3} 1.12×10^{-2}	1.83×10^{-2} 1.33×10^{-1}	1.97×10^{-1} 1.37
0.005	1.50×10^{-3} 1.12×10^{-2}		1.68×10^{-2} 1.22×10^{-1}	1.96×10^{-1} 1.36
0.05	1.83×10^{-2} 1.37×10^{-1}	1.68×10^{-2} 1.26×10^{-1}		1.78×10^{-1} 1.23
0.5	2.01×10^{-1} 1.39	2.00×10^{-1} 1.38	1.81×10^{-1} 1.22	

[a] All numbers are percentages. The first number is the relative percentage deviation at the maximum z velocity. The second number is the relative percentage average deviation as described in the text.

intended to cover the parameter range of a number of zone-broadening experiments reported previously in the literature. These include the experiments of Tallarek, Bayer, and Guiochon,[29] given as simulations 1 and 2, in which 9- and 50-μm particles were utilized, and the experiments of Magnico and Martin,[22] given as simulation 3, where 210-μm particles were employed. The diffusion coefficient of a small unretained tracer solute ($D = 8.00 \times 10^{-6}$ cm^2 s^{-1}) is used for all three simulations. Note that, in all cases considered here, the Reynolds number, given as $\mathrm{Re} = vd/\eta$, where η is the kinematic viscosity, is less than 0.5. The value of η used in the conditions given in Table 1 is 0.01 cm^2 s^{-1} which is approximately that of water. For each simulation, either 10 000 particles (for $\nu < 55$) or 100 000 particles (for $\nu > 55$) are used. We use more particles as the zones get wider. In all cases, the channel length L is 0.01 m and the step length per each iteration is 10^{-8} m. The run time for one velocity simulation with 100 000 particles is ≈16 h.

RESULTS AND DISCUSSION

Velocity Rescaling. In this section, we present an error analysis of the velocity rescaling step. As discussed previously, velocity rescaling simplifies the study by using only one calculated flow field and then rescaling for different velocities. In this study, a 1000-particle packed bed in a periodic cube ($\epsilon = 36\%$) is resolved with 256 grid points per side. The flow velocities are calculated using the LB technique for Reynolds numbers of 0.001, 0.005, 0.05, and 0.5. Next, the axial (z) velocities are scaled through multiplication by the ratio of Reynolds numbers. The error is then tabulated in two ways. The first of these, shown as the first entry in the matrix elements of Table 2, is the relative deviation between the scaled and unscaled flow field at the location of maximum velocity. This number, expressed as a percentage, is given by

$$E_1 = \sqrt{\frac{(v_2' - v_1')^2}{v_1'^2}} \times 100 \qquad (9)$$

where v_1' is the maximum velocity of the unscaled flow field and v_2' is the maximum velocity of the scaled flow field. The second number given in the matrix of entries in Table 2 is the biased average relative deviation, expressed as a percentage, so that

$$E_2 = \sqrt{\frac{\sum\left(\frac{(v_2 - v_1)^2}{v_1^2}\right)}{N' - 1}} \times 100 \qquad (10)$$

where v_1 and v_2 are the original and rescaled velocities and N' is the number of velocities. The sum is taken over all N' velocities whose value is greater than or equal to 10^{-4} of the maximum velocity in the flow field. This is done because very small velocities show greater relative error between scaled and unscaled flow fields. By not including all of the velocities in the flow field, these results are biased but more useful because the velocities below $10^{-4}v_{max}$ contribute nothing but molecular diffusion to the dispersion mechanism. The velocities that are not included in the sum given in eq 10 are ≈1% of the grid points in the flow field.

The results given in Table 2 show that all velocities can be derived from one flow field with errors typically below 0.2% for the maximum relative velocity and below 1.5% in the biased relative average velocity over the Reynolds number range of interest. If the range of velocities used in the sum of eq 10 is restricted to $\geq 10^{-2}v_{max}$, the biased average relative deviation is ≈100 times smaller. Furthermore, the results in Table 2 show that the error is close to symmetrical. For example, the error found for rescaling at $Re = 0.001$ to $Re = 0.5$ is very similar to the error incurred when rescaling at $Re = 0.5$ for use at $Re = 0.001$. This is an expected result. These results are generally consistent with earlier work[43] where it was found that the apparent permeability of a packed bed remains relatively constant for $Re < 2$. These results suggest that for $Re \leq 0.5$ velocity rescaling can be used with little error. This simplifies the computational methodology greatly by allowing us to use one flow field for all of the velocities when zone broadening is studied as a function of velocity.

Peak Shape. The resulting arrival time histograms of two of the simulations for the 50-μm particle packs are shown in Figure 3 for $\nu = 25$ and $\nu = 62.5$. These appear to be very close to Gaussian and show good smoothness of sampling without digital filtering, which has been utilized in the past[80] for these types of simulations in open tubes. Moment analysis reveals that these peaks do have a nonzero skew (i.e., finite third moments). This is expected for any flow system system because more diffusive broadening takes place for the later eluting part of the zone as compared with the earlier eluting part.[74,81] The usual sources of nonsymmetrical peaks such as slow mass transport from particle to liquid and instrumental injection effects are absent from this simulation. Hence, the zones would be expected to be nearly Gaussian and this is the case for lower and higher velocities.

(80) Schure, M. R. *Anal. Chem.* **1988**, *60*, 1109−1119.
(81) Jönsson, J. Å. *Chromatographia* **1984**, *18*, 427−433.

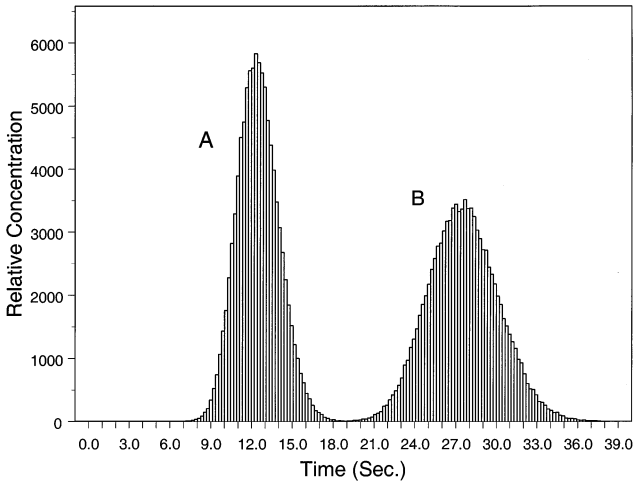

Figure 3. Arrival time histograms for simulation of the 50-μm particle pack for (A) $\nu = 62.5$ and (B) $\nu = 25$.

Low-Velocity Simulations. The results of the simulations for the dimensional plate height, H, as a function of the average fluid velocity is shown in Figure 4A for the three particle sizes under nonretentive conditions. Figure 4B gives the same results in terms of the nondimensional plate height, h, and the nondimensional average fluid velocity. The results in Figure 4 are for $\nu < 55$, the typical velocity range for analytical separations. We show this separately from the higher velocity data to compare models that have been previously compared with lower velocity data.

Two results appear immediately. First, the different particle diameter simulation data in the nondimensional plot appear to collapse to a single curve. This lends credence to the idea that the "reduced" plate height is, in fact, correctly nondimensionalized.[7,82,83] Since the particle packing of the simulations is exactly the same for the three different particle sizes, and the particles are perfectly monodisperse, this type of experiment is impossible to conduct in a laboratory. Second, the minimum plate height, h_{min}, is found to be ≈0.99 at $\nu \approx 5.00$. The simulation data given here agree reasonably well with experiment. For example, Magnico and Martin[22] found that $h_{min} \approx 1$ at $\nu \approx 3$. Using pulsed field gradient nuclear magnetic resonance (PFGNMR) techniques, Tallarek, Bayer, and Guiochon[29] found $h_{min} = 0.94$ at $\nu \approx 3.1$. Other experimental data yield a higher ν at the minimum; for example, data presented in refs 83 and 84 exhibit a minimum closer to 6. However, this is for porous particles, where pore diffusion should increase the term that is linear in velocity and should thus move the point at which h_{min} occurs to lower velocity.[20] The precision in obtaining the location of the h_{min} velocity is poor because the minimum is generally shallow. Furthermore, even small amounts of retention will have an effect on the velocity value where h_{min} is found.

The elution time of the zones, t_e, although not listed here, are very close to that expected from L/v_z. At higher velocity, typically $\nu > 50$, $t_e < L/v_z$ with deviation >10%. This is due to the lack of statistical sampling of all streamlines by the solute. The zones are still close to Gaussian at the higher velocities. For example, the 9-μm simulations show efficiencies in excess of 200 plates at $\nu > 150$. Near-Gaussian zone shapes are noted to occur with

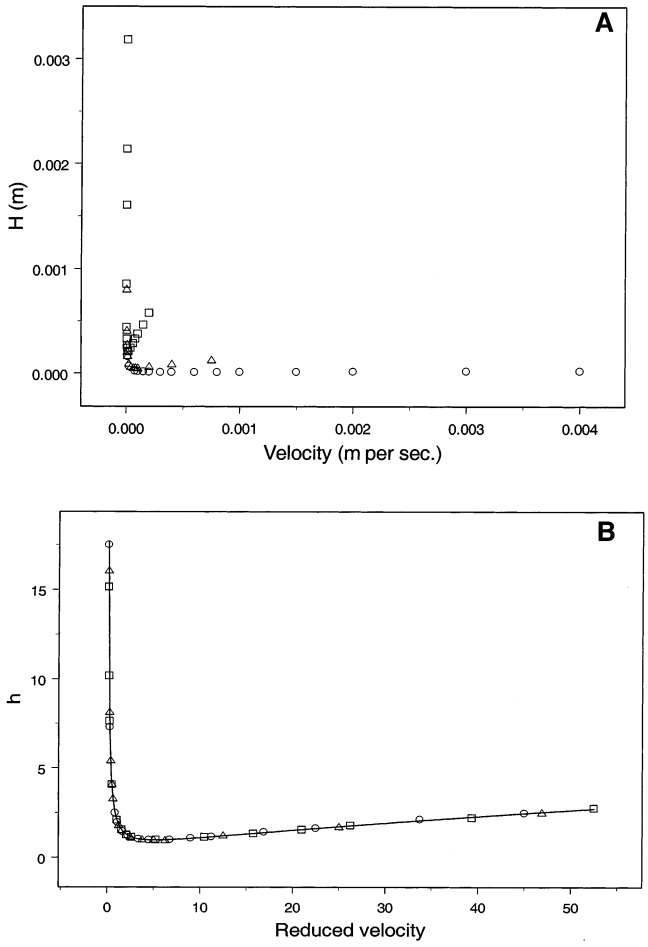

Figure 4. (A) Dispersion as measured by the dimensional plate height H as a function of the average dimensional fluid velocity for $\nu < 55$. The particle diameters are 9- (circles), 50- (triangles), and 210-μm (square) particles. (B) Nondimensional plate height h as a function of the reduced (nondimensional) average fluid velocity for $\nu < 55$. The solid curve is the best curve fit using the G5 model.

efficiencies in excess of 25 plates, and this has been discussed in the literature.[58,85] The simulations reported here were designed to have efficiencies that were high enough to minimize transient zone effects where non-Gaussian zone shapes are present.[58]

The results of least-squares curve fits of the $\nu < 55$ data are given in Table 3 and Figure 5 for the seven different models tested. The best fit of the simulation data from the models is given by the four-parameter Knox model (K4) followed by the five-parameter Giddings model (G5). These two curves are essentially indistinguishable in Figure 5. The three-parameter van Deemter model (vD3) is the poorest fitting model and appears not to capture the mechanical dispersion mechanism. The Giddings four-parameter model (G4) is shown to give almost as good results as the Giddings five-parameter model (G5).

The best fitting models (G5 and K4) have velocity exponents of ≈0.6 in the mechanical dispersion term for the $\nu < 55$ data. This is at variance with the Giddings four-parameter model, where the velocity exponent n in eq 6 is unity, and with the three-parameter Knox equation, where $n = 0.33$. Another observation is that the tortuosity factor γ in eq 6 is very close to unity from the parameter estimates. This term is related to the diffusional

(82) Giddings, J. C. *J. Chromatogr.* **1964**, *13*, 301−304.
(83) Done, J. N.; Knox, J. H. *J. Chromatogr. Sci.* **1972**, *10*, 606−612.
(84) Unger, K. K. *J. Chromatogr.* **1978**, *149*, 1−12.
(85) Fellinger, A. *Data Analysis and Signal Processing in Chromatography*; Elsevier Publishing: New York, 1998.

Table 3. Least-Squares Parameter Estimate Analysis for $\nu < 55$

model	RSD[a] (%)	parameter 1	2	3	4	5
G4	1.75	$\gamma = 0.995$	$\lambda = 0.429$	$\omega = 5.31$	$c = 0.0367$	
G5	1.46	$\gamma = 0.992$	$\lambda = 5.62$	$\omega = 56.9$	$c = 0.0156$	$n = 0.612$
H4	2.07	$\gamma = 0.990$	$\lambda = 63800$	$\omega = 598000$	$c = 0.0222$	
HL4	3.57	$\gamma = 0.985$	$\lambda = 12600$	$\omega = 106000$	$c = 0.0357$	
vD3	6.71	$a = 0.301$	$b = 1.94$	$c = 0.0493$		
K3	3.31	$a = 0.238$	$b = 1.97$	$c = 0.0357$		
K4	1.46	$a = 0.205$	$b = 1.98$	$c = 0.00535$	$n = 0.621$	

[a] Relative standard deviation.

Table 4. Least-Squares Parameter Estimate Analysis for the Complete Velocity Range

model	RSD[a] (%)	parameter 1	2	3	4	5
G4	8.21	$\gamma = 0.999$	$\lambda = 2.49$	$\omega = 61.9$	$c = 0.00940$	
G5	1.42	$\gamma = 0.994$	$\lambda = 21.6$	$\omega = 226$	$c = -0.00611$	$n = 0.713$
H4	8.68	$\gamma = 0.983$	$\lambda = 4.57 \times 10^7$	$\omega = 2.67 \times 10^8$	$c = 0.00358$	
HL4	12.8	$\gamma = 0.967$	$\lambda = 5.37 \times 10^7$	$\omega = 2.20 \times 10^8$	$c = 0.012$	
vD3	21.6	$a = 0.906$	$b = 1.82$	$c = 0.0207$		
K3	13.6	$a = 0.512$	$b = 1.94$	$c = 0.0119$		
K4	1.44	$a = 0.209$	$b = 1.99$	$c = -0.0287$	$n = 0.756$	

[a] Relative standard deviation.

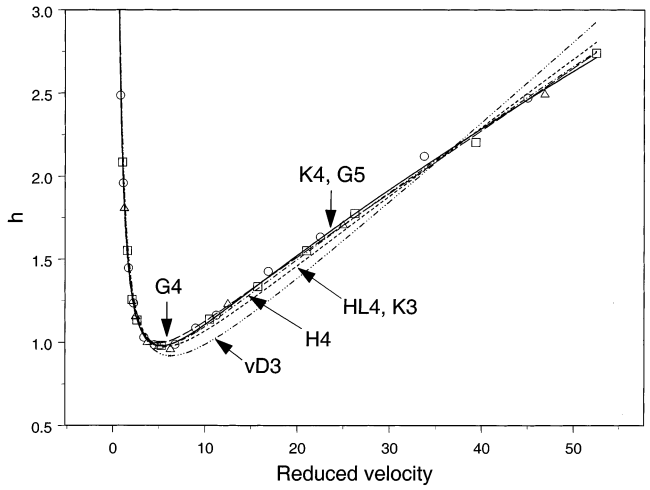

Figure 5. Curve fits of the models to the nondimensional low-velocity data for $\nu < 55$. The particle diameter legend is the same as the caption to Figure 4.

characteristics of molecules in the tortuous interstitial regions of the packing. Simulation studies have examined diffusion of pointlike molecules in porous, noninteracting media and concluded[86] that tortuous geometry, like that found in the interstitial regions of a nonporous packed bed, does not affect the rate of mass transport in the fluid phase. Hence, γ should be unity, and the parameter estimation of the models G4, G5, H4, and HL4, which have a term of $2\gamma/\nu$, shows γ very close to 1 in Table 3.

The λ and ω parameter estimations in Table 3 appear to be faulty for the four-parameter Huber model and the Horváth−Lin models because of the very large magnitudes that are obtained. The values of λ and ω for these models show a distinct inability of the curve fitting to obtain independent parameters. This is typically a sign in parameter estimation that the model is incorrect.[87] Parameter estimation of the G4, G5, H4, and HL5 models is difficult because the λ and ω terms appear from inspection of eq 6 to lack independence. This can happen when the data to be fit do not include enough of the characteristic shape of the model; for example, trying to fit a Langmuir isotherm[58] to only the flat part of an isotherm. As shown below, the λ and ω values are estimated to have different values when the full curves are utilized. In that regard, the models do not fit well unless a larger characteristic region of the data is sampled, as in the larger velocity parameter estimations given in Table 4.

Tallarek, Bayer, and Guiochon[29] estimated $\lambda = 1.46$ and $\omega = 20.71$ from PFGNMR data while elution data gave $\lambda = 2.62$ and $\omega = 11.38$ using the Giddings model G4. Furthermore, Magnico and Martin[22] gave values of $\lambda = 0.53$ and $\omega = 10.3$ (they estimated γ to be 0.6). Reasonable agreement of λ from the simulation data in Table 3 for the G4 model with the value of Magnico and Martin[22] is noted. However, simulation gives $\omega = 5.31$ and Magnico and Martin[22] gave $\omega = 10.3$, which differs by a factor of $\approx$2. As discussed previously,[29] the interpretation of λ and ω may contain considerable uncertainty. In all cases given in Table 3 except the van Deemter model, the nonequilibrium or Taylor dispersion term c is estimated to be very small. Even for retentionless zones, Taylor dispersion contributes to zone broadening; hence, the c term should not be zero under these conditions.

Complete Velocity Range. The complete h versus ν data are shown in Figure 6 along with the curve fits from the various models. The coefficients for these curve fits are given in Table 4. The results are qualitatively similar to those given in Figures 4 and 5 and Table 3. However, a number of important differences exist and these will now be discussed. First, the bending over of

(86) Malek, K.; Coppens, M.-O. *Phys. Rev. Lett.* **2001**, *87*, 125505-1−125505-4.

(87) Ratkowsky, D. A. *Handbook of Nonlinear Regression Models*; Marcel Dekker: New York, 1990.

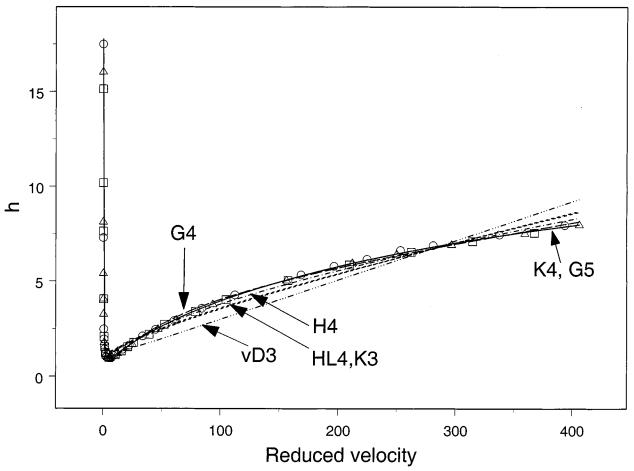

Figure 6. Curve fits of the models to the nondimensional velocity data over the full velocity range. The particle diameter legend is the same as the caption to Figure 4.

the data is now clearly evident for higher velocities where mechanical dispersion effects become significant. This has an interesting effect in the parameter estimates, yielding values of λ and ω that are larger than those shown in Table 3. However, the four-parameter Knox model and the five-parameter Giddings model fit the data exceedingly well. The Huber model (H4), which has a $^1/_2$ power dependence on velocity, does approximately as well as the Giddings four-parameter model, which has a linear velocity dependence, in fitting the data. This is important because it suggests that the sensitivity to fitting the data when the exponential dependence on velocity is varied is not very high. This has been discussed by Magnico and Martin.[22] Also note that the Horváth and Lin model fits the simulation data about as well as the three-parameter Knox model.

In both the K4 and G5 models, there is a clear difference in fitting as compared with the other models. The exponents are now 0.713 for G5 and 0.756 for K4. This suggests that the scaling of ν^{-1} in the coupling term may be approximate. Furthermore, the c values being negative are simply noise in curve fitting and simulation data; this parameter should be small but finite, as discussed above. Negative c values are not physically meaningful.

The origin of this noninteger exponent has been attributed to[21] the $\nu \ln \nu$ scaling of dispersion predicted by Koch and Brady[88] for diffusive boundary layer movement of solute around the particle. However, studies of tracer dispersion in porous media using simulation techniques[47] have not found this scaling for $\nu <$ 1000. Rather, it has been suggested[47] that the region $10 \lesssim \nu \lesssim$ 1000 is a transition region between diffusive dispersion and pure mechanical dispersion,[88] which dominates for $\nu \gtrsim 1000$. In this regard, a noninteger scaling would not be surprising, and this has been observed in other studies.[21] The variability of this exponent with different packing porosity, and the effect of retention on zone broadening, will be studied in the future by the simulation method presented in this paper.

Regardless of the origin of this effect, the simulations yield zone-broadening data in this velocity region that are in agreement with experiment. The models can fit h in this velocity region very well when noninteger velocity scaling is allowed. The simulations appear to capture the essential dynamics of the flow processes involved in packed-bed chromatography.

(88) Koch, D. L.; Brady, J. F. *J. Fluid Mech.* **1985**, *154*, 399−427.

Future Studies. In the LB flow simulation, each grid point is identified as either solid or nonsolid. The convection−diffusion−retention simulation is set up so that a solid particle region is defined as a spatial region where the eight grid points of a cube are all denoted to be solid. Otherwise the rectangular region is on the surface if some of the points are "solid". The region is completely in the fluid if none of the vertex points are marked as solid. In this way, the convection−diffusion−retention algorithm is independent of the particle geometry so that *any* particle shape can be modeled. For example, spheres, cubes, toroids, and any other solid geometries do not require specification of the particle shape during the simulation. In this regard, this type of simulation is ideal for studying complex media such as monolithic column materials[89,90] where the geometry is not constant nor isolated. We have examined monolithic materials, and simulation studies of this type will be conducted in the future.

Random packing of chromatographic particles is expected when the traditional packing methods are employed. However, advanced colloidal crystallization[91] and templating technologies[92] may allow the preparation of crystalline lattices of spheres or periodic holes to be synthesized. These could be easily studied using this type of simulation because these flows are periodic and would require little more than one unit cell of media for simulation. The experimental chromatographic consequences of these packings are not known, but some studies of the fluid mechanics have been made using experimental,[93] theoretical,[94] and simulation[47] approaches.

Modeling porous particles, for which there is no appreciable convection in the pore, can be easily accommodated. The stochastic functions of waiting times, obtained from an independent simulation of porous particles with no flow, are added to each particle elution time. This is done as a postprocessing step in exactly the same way as retention is added. This scheme works fine except when the flow field either exists within the particle or the presence of the particle pores affects the flow field. The case when the flow field is nonzero within the particle is extremely demanding on computer resources because the computational grid must be fine enough to contain detailed pore structure and yet large enough to cover enough of the particle pack so as to reproduce the mechanical dispersion from interparticle effects correctly. The extent to which these two length scales can be bridged into separate simulations is an open question, although a semiempirical approach to this problem was recently reported.[95]

We have shown how simulation can be utilized to study packed-bed chromatography with a monodisperse packed bed of particles. Many studies have been conducted on beds of mixed particle size. Quantifying zone broadening in this case is difficult because the fluid mechanics depends on how the particles pack. Simple analytical theories that describe zone broadening are nearly impossible to construct. With the type of simulation described in

(89) Peters, E. C.; Petro, M.; Svec, F.; Fréchet, J. M. J. *Anal. Chem.* **1997**, *69*, 3646−3649.
(90) Lubda, D.; Cabrera, K.; Kraas, W.; Schaefer, C.; Cunningham, D. *LCGC* **2001**, *19*, 1187−1191.
(91) Velev, O. D.; Jede, T. A.; Lobo, R. F.; Lenhoff, A. M. *Nature* **1997**, *389*, 447−448.
(92) Velev, O. D.; Jede, T. A.; Lobo, R. F.; Lenhoff, A. M. *Chem. Mater.* **1998**, *10*, 3597−3602.
(93) Gunn, D. J.; Pryce, C. *Trans. Inst. Chem. Eng.* **1969**, *47*, T341−T350.
(94) Koch, D. L.; Cox, R. G.; Brenner, H.; Brady, J. F. *J. Fluid Mech.* **1989**, *200*, 173−188.
(95) Kandhai, D.; Hlushkou, D.; Hoekstra, A. G.; Sloot, P. M. A.; Van As, H.; Tallarek, U. *Phys. Rev. Lett.* **2002**, *88*, 234501-1−234501-4.

this paper, once the particles are packed and the flow field constructed, the zone broadening is obtained in the same way as for a monodisperse particle study. This type of study is now underway in our laboratory for various ratios of particle sizes and for distributions of particle sizes.

Electrochromatography, where flow is produced by electroosmosis instead of pressure-driven flow, can also be studied using this type of simulation technique. In this case, the LB technique must be modified to incorporate different boundary conditions. We are presently exploring the feasibility of this using the thin double-layer approximation,[96,97] where the flow is finite at the particle surface.

Another area of interest for packed-bed simulation is that of packed cylindrical tubes where the number of particles in the cross section is relatively small. In this case, wall effects[34,43,98,99] become a significant part of the flow field, leading to modified behavior. Although some experimental data may exist regarding these effects, it is exceedingly difficult to study these systems because they are difficult to prepare in a reproducible way.

In the study discussed in this paper, the minimum reduced plate height is very close to unity. Other sources of zone broadening such as nonuniform zone introduction and bed inhomogenieties are known to exist. The absence of these effects from the simulation may be what causes h_{min} to be near unity as opposed to higher values found in typical experimental columns. These effects all lend themselves to the type of study using the simulation methodology outlined in this paper.

We believe that this form of simulation opens new routes of investigation into new media behavior and as a test bed to solve many older unresolved problems in packed-column performance and efficiency. Although the present simulation technology requires a moderately large computer system to be effective, we expect this technology to be routinely available within a decade and to open further vistas into packed-bed chromatographic technology.

ACKNOWLEDGMENT

We appreciate a large amount of computing resources that have been generously given by the Minnesota Supercomputer Institute and the University of Minnesota. D.M.K. acknowledges support from the National Science Foundation under Grant DMR-0083219, and the donors of the Petroleum Research Fund, administered by the American Chemical Society. R.S.M.'s work was sponsored in part by the Army High Performance Computing Research Center under the auspices of the Department of the Army, Contract DASW01-01-C-0015. The content does not necessarily reflect the position or the policy of the government, and no official endorsement should be inferred. Support from the National Science Foundation under Grant CHE-0213387 is gratefully acknowledged by M.R.S. as is the support of the Rohm and Haas Company.

NOMENCLATURE

GLOSSARY

a	mechanical or eddy dispersion coefficient
$a_{0,u} - a_{7,u}$	velocity interpolation coefficients
b	model coefficient for lumped diffusion and mechanical dispersion
c	resistance to mass transport coefficient
d	packing particle diameter
D	diffusion coefficient
E_1	relative deviation of velocity scaling in the maximum velocity
E_2	biased relative average deviation in velocity scaling
h	nondimensional (reduced) plate height
h_{min}	minimum nondimensional (reduced) plate height
H	plate height
L	length of packed-bed simulation
M_1	first moment
M_2	second moment
n	exponents in zone-broadening models
N	number of solute particles used in simulation
N'	number of velocity field grid points used in eq 10
t	time
t_e	elution time
t_s	time step
t_s'	truncated time step for movement to and from surface
t_i	arrival time of the ith solute particle
u	generalized coordinate; either x, y, or z coordinate
$\bar{u}$	average diffusion distance
u_i, u_{i+1}	generalized coordinate at the ith and ith + 1 iteration
v	mean axial velocity
v_x	velocity in the x direction
v_y	velocity in the y direction
v_z	velocity in the z direction
v_1	axial velocity of the unscaled flow field
v_1'	maximum axial velocity of the unscaled flow field
v_2	axial velocity of the scaled flow field
v_2'	maximum axial velocity of the scaled flow
v_{max}	maximum velocity
x	the x coordinate
y	the y coordinate
z	the z coordinate
γ	tortuosity factor
ϵ	porosity
η	kinematic viscosity
λ, ω	coupling model geometric parameters
ν	Péclet number or reduced velocity
ϕ	volume fraction of solids
σ	standard deviation of Gaussian density function
l	distance to particle surface

(96) Kozak, M. W.; Davis, E. J. *J. Colloid Interface Sci.* **1989**, *127*, 497−510.
(97) Coelho, D.; Shapiro, M.; Thovert, J. F.; Adler, P. M. *J. Colloid Interface Sci.* **1996**, *181*, 169−190.
(98) Mueller, G. E. *Chem. Eng. Sci.* **1991**, *46*, 706−708.
(99) Schnitzlein, K. *Chem. Eng. Sci.* **1993**, *48*, 811−815.

Received for review June 21, 2002. Accepted September 19, 2002.

AC0204101